ADVANCED FUNCTIONAL MATERIALS

www.afm-journal.de

Light-Induced Surface Modification of Natural Plant Microparticles: Toward Colloidal Science and Cellular Adhesion Applications

*Ee-Lin Tan, Michael G. Potroz, Gaia Ferracci, Joshua A. Jackman, Haram Jung, Lili Wang, and Nam-Joon Cho**

Playing an instrumental role in the life of plants, pollen microparticles are one of the most fascinating biological materials in existence, with abundant and renewable supply, ultrahigh durability, and unique, species-specific architectural features. Aside from their biological role, pollen microparticles also demonstrate broad utility as functional materials for drug delivery and microencapsulation, and increasingly for emulsion-type applications. As natural pollen microparticles are predominantly hydrophobic, developing robust surface functionalization strategies to increase surface hydrophilicity would increase the range of colloidal science applications, including opening the door to interfacing microparticles with biological cells. This research investigates the extraction and light-induced surface modification of discrete pollen microparticles from bee-collected pollen granules toward achieving functional control over the responses elicited from discrete particles in colloidal science and cellular applications. Ultraviolet–ozone treatment is shown to increase the proportion of surface elemental oxygen and ketones, leading to increased surface hydrophilicity, enhanced particle dispersibility, tunable control over Pickering emulsion characteristics, and enhanced cellular adhesion. In summary, the findings demonstrate that light-induced surface modification improves the functional properties of pollen microparticles, and such insights also have broad implications across materials science and environmental science applications.

1. Introduction

The discovery and use of natural materials for formulating microparticle-based Pickering emulsions are of significant interest for a wide range of industrial applications.[1–12] Pollen particles represent an ideal source of natural microparticles for use in developing microparticle-stabilized Pickering emulsion systems. Pollens exhibit numerous desirable properties for functional emulsion applications, such as particle monodispersity,[13] physicochemical robustness,[14] amphiphilicity,[15] biocompatibility,[16] and diverse surface chemistry options for functionalization and compound binding.[17–23] In general, there is growing interest in utilizing pollen microparticles for a wide range of applications, such as the extraction of pollen shells for microencapsulation and drug delivery applications.[24–30] Although, sporoderm microcapsules have been shown to offer a wide range of potential benefits, they typically rely on harsh chemical extraction protocols, and are limited by requiring additional regulatory approval for use in oral delivery applications. In contrast, natural pollens have the advantages of requiring minimal processing, and are considered to be regulation-free for human consumption and topical applications.[31,32]

Pollen represents an ideal microparticle for developing natural Pickering emulsion systems for use in a wide range of applications. First, pollen microparticles exhibit a spectrum of hydrophobic and hydrophilic properties with a high degree of particle uniformity and monodispersity.[33] Second, bee-collected pollens are available in industrial-scale quantities and are competitively priced in comparison to other natural materials, which may be used as microparticles, such as celluloses and waxes.[34,35] Third, bee-collected pollens have a long history of use as food and medicine across a wide range of cultures with extensive published research supporting numerous health benefits, and are widely available.[36–38] Overall, discrete pollen particles extracted from bee-collected pollens present an ideal source of microparticles for stabilizing oil and water systems in applications as diverse as foods, therapeutics, cosmetics, and paints, while overcoming potential regulatory hurdles associated

E.-L. Tan, Dr. M. G. Potroz, G. Ferracci, Dr. J. A. Jackman, H. Jung, Prof. N.-J. Cho
School of Materials Science and Engineering
Nanyang Technological University
50 Nanyang Avenue 639798, Singapore
E-mail: njcho@ntu.edu.sg

E.-L. Tan, Dr. M. G. Potroz, G. Ferracci, Dr. J. A. Jackman, H. Jung, Prof. N.-J. Cho
Centre for Biomimetic Sensor Science
Nanyang Technological University
50 Nanyang Drive 637553, Singapore

Prof. L. Wang
State Key Laboratory on Integrated Optoelectronics
College of Electronic Science and Engineering
Jilin University
Changchun 130012, P. R. China

Prof. N.-J. Cho
School of Chemical and Biomedical Engineering
Nanyang Technological University
62 Nanyang Drive 637459, Singapore

The ORCID identification number(s) for the author(s) of this article can be found under https://doi.org/10.1002/adfm.201707568.

DOI: 10.1002/adfm.201707568

with the ingestion and topical application of many other highly processed compounds. In particular, previous studies have highlighted the potential for compound loading directly into natural pollens,[39–41] and thereby, discrete pollen particles may provide a key platform technology for enhancing and modernizing the extensive field of traditional herbal therapeutics.[42,43]

Understanding and tuning the interfacial properties of discrete pollen particles is crucial to ensure the effective utilization of pollen for developing functional oil/water-based formulations. Bee-collected pollens are bound into millimeter-sized granules by a complex mixture of bee salivary gland secretions, nectars, and pollenkitt on the pollen surface.[44] During the process of extracting discrete pollen particles, water soluble and lipidic compounds are removed, exposing the native pollen outer-shell biopolymer, sporopollenin. Sporopollenin is generally considered to be an amphiphilic complex biopolymer,[33,45] with variations in composition between plant species.[46,47] Acid-extracted and natural sporopollenin-based plant spores from *Lycopodium clavatum* have been shown to stabilize oil and water emulsion systems, and the stabilization mechanism has been attributed to the Janus structure of the particles.[33,45] However, Pickering emulsion studies have yet to be undertaken with pollen, and to further develop the utility of pollen-based microparticle-stabilized Pickering emulsion formulations, a facile means to tune the wetting potential and/or surface chemistry of pollen is of significant interest. Various chemical derivatization methods have been explored for surface functionalization of *L. clavatum* sporopollenin, such as amination, halogenation, azidation, thiolation, sulfurylation, and phosphorylation, although these methods typically require additional harsh reagents and multiple processing steps.[18,20] Plasma treatment of *L. clavatum* spores has been shown to enhance wetting and dispersion properties in pure aqueous environments.[48] However, ultraviolet–ozone (UV–O) treatment is a more easily implementable surface modification process, which also leads to improved surface wetting of polymers,[49] and potential enhancements in polymer/cell adhesion.[50,51] Studies with polymer microparticles have shown UV–O treatment to easily and successfully modify the chemistry and interfacial properties of polystyrene and polycaprolactone microparticles leading to improved wetting, particle self-assembly, polymer binding, and particle/cell adhesion.[52–54]

A greater understanding of the influence of UV–O on pollen sporopollenin chemistry has implications for numerous fields of research. The pollen outer shell is known to provide ultraviolet (UV) protection for sensitive genetic material. Cinnamic acids present in the outer shell are responsible for UV absorption, and quantifying the proportion of cinnamic acids is used as a means for studying climate change from pollen shells in fossil records.[55,56] There is interest in the influence of ozone as an environmental pollutant on pollen properties.[57,58] Pollen surface acidity is expected to increase from ozone exposure, and the acidity of the germination environment is known to influence the germination potential of pollen.[59] It has also been proposed that pollen exposed to ozone may alter pollen–human cell interactions,[60] and thereby impact pollen allergenicity or immunomodulatory properties.[61] However, to our knowledge, there are no studies that have attempted to elucidate the impact of UV/ozone treatment on sporopollenin chemistry or translated such knowledge into interfacial science-driven applications.

Herein, we explored the extraction and UV–O surface modification of bee-collected *Camellia sinensis* pollen for developing Pickering emulsion-based formulations and enhancing pollen/cell adhesion properties (**Figure 1**). *C. sinensis* is a species of plant used for the production of tea, and has been shown to exhibit numerous health benefits and is used in numerous well-being products.[62] Washing and defatting of raw bee-collected pollen granules were conducted to obtain discrete pollen particles. Pollen morphological properties were analyzed to determine the degree of particle purity and monodispersity. UV–O treatment of defatted-pollen was conducted and the basic wetting properties of UV–O treated pollen were analyzed. Analysis of surface elemental composition and chemical binding were conducted to elucidate the effect of UV–O treatment. Properties of pollen particle aqueous suspensions and Pickering emulsions were explored with both untreated and UV–O treated pollen. Finally, pollen/cell adhesion properties were explored with both untreated and UV–O treated pollen and Huh-7.5 liver hepatocarcinoma cells.

2. Results and Discussions

2.1. Extraction of Pollen from *C. sinensis* Bee Pollen Granules

Defatting and washing of bee pollen granules removed various surface adhered residues and produced free-flowing discrete particles. Bee pollen washing and defatting was carried out to remove surface adhered organic materials and dust or other particulate matter that may be present in the raw bee pollen (Figure S1, Supporting Information). After the defatting and drying processes, bee pollen pellets produced loose pollen powder, with a weight yield of 42.6 ± 0.9%, and changed in color from light orange to pale yellow (**Figure 2**a and Figure S2, Supporting Information). The change in color may be attributed to the removal of surface wax and nectar.[63] Dynamic imaging particle analysis (DIPA) indicated that the resulting loose defatted *C. sinensis* pollen powder exhibited 99.3 ± 0.5% purity of pollen species, was highly monodispersed with a particle size of 36.2 ± 1.8 µm (Figure S3, Supporting Information), and comprised 31 204 ± 3390 particles per milligram with a particle weight of 32.0 ± 3.5 ng.

2.2. UV–O Exposure Effect on Pollen Surface Chemistry

2.2.1. Surface Morphology and Wetting Properties

UV–O treatment of defatted pollen resulted in smoothing of the pollen surface and increased pollen wetting. Defatted pollen samples were treated with UV–O for 15, 30, 60, and 120 min. From scanning electron microscopy (SEM) images collected, UV–O treatment did not result in significant morphological changes of pollen (Figure 2b and Figure S4, Supporting Information); however, surface smoothing was observed at the nanoscale (Figure 2c). Contact angle measurements indicated that the contact angle decreases with increasing exposure to UV–O but stabilizes beyond 30 min treatment (Figure 2d), with 0, 15, 30, 60, and 120 min UV–O resulting in contact angles of 128.4 ± 4.3°, 87.2 ± 1.1°, 58.8 ± 4.1°, 51.1 ± 1.5°, and

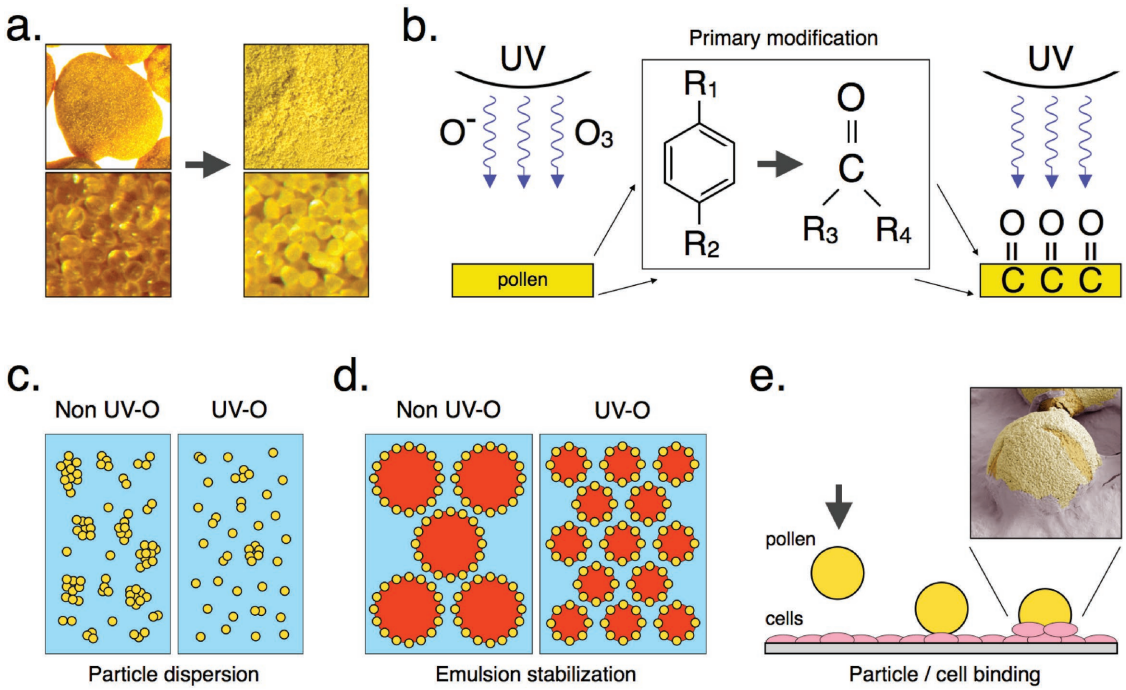

Figure 1. Schematic diagram showing pollen extraction and surface modification, resulting in tuning of wetting properties, emulsification potential, and particle/cell adhesion: a) Extraction of discrete pollen particles from bee-collected pollen granules; b) ultraviolet–ozone (UV–O) treatment of defatted pollen particles resulting in the opening of aromatic rings with the formation of $R_2C{=}O$ bonds and increased overall oxygen content; c) tuning of wetting and aqueous suspension properties; d) tuning of microparticle Pickering emulsion properties; and e) tuning of particle/cell adhesion for pollen binding with liver hepatocarcinoma cells.

55.0 ± 4.4°, respectively. The lack of changes in macroscale pollen morphology suggests that the reduction of the contact angle with UV–O treatment may be primarily attributed to modification of surface chemistry.

2.2.2. Pollen Surface Elemental Composition and Binding Profiles

Surface chemistry analysis of untreated and UV–O treated pollen indicated increases in the proportion of elemental oxygen attributable to increases in the proportion of ketone ($R_2C{=}O$) binding. Wide scan X-ray photoelectron-spectra (XP-spectra) highlight the presence of oxygen (O1s) and carbon (C1s) peaks, with an increase in the O1s peak and a decrease in the C1s peak between 0 and 120 min UV–O treatment (**Figure 3**a and Figure S5, Supporting Information). Overall, the total proportion of elemental oxygen increased from 0 to 120 min UV–O, with 0, 15, 30, 60, and 120 min UV–O treatment resulting in an atomic oxygen concentration of 20.7 ± 0.4%, 21.7 ± 0.1%, 23.0 ± 0.1%, 24.9 ± 0.1%, and 28.0 ± 0.3%, respectively (Figure 3b). The proportion of elemental carbon decreased relative to the increases in oxygen.

Peak fitting analysis of C1s and O1s peaks for untreated and 120 min UV–O treated pollen was used to examine the shifts in proportions of carbon and oxygen bond types. For the carbon binding (C1s) peak, carboxylic acid/ester ($RO{-}C{=}O$), $R_2C{=}O$, carbon-oxygen (COR), and carbon-carbon/carbon-hydrogen (CC/CH) binding were assigned to binding energies of 289.0, 288.0, 286.3, and 284.9 eV,[64] respectively (**Table 1**, Figure 3c, and Figure S6, Supporting Information), and UV–O treatment resulted in decreases in $RO{-}C{=}O$ binding, increases in $R_2C{=}O$ binding, and minimal changes in COR and CC/CH binding. For the oxygen binding (O1s) peak, $RO{-}C{=}O$, COR, and $R_2C{=}O$ binding were assigned to binding energies of 534.1, 532.7, and 531.6 eV,[64] respectively, and UV–O treatment resulted in decreases in $RO{-}C{=}O$ binding, increases in $R_2C{=}O$ binding, and minimal changes in COR binding. Collectively, shifts in the proportion of oxygen binding were similar for both C1s and O1s binding, with an ≈57% decrease in COOR bonds, an ≈2% proportional increase for COR bonds, and an ≈78% increase in $R_2C{=}O$ bonds (Figure 3d). Relating both of increases in total oxygen % and changes in oxygen binding proportions it is possible to depict total oxygen binding distributions (Figure 3e). At 0 min UV–O, the total oxygen content of the surface is 20.7 ± 0.4%, with COR, $R_2C{=}O$, and $RO{-}C{=}O$ binding proportions of 12.5 ± 2.3%, 4.9 ± 0.9%, and 4.6 ± 0.8%, respectively. Whereas, at 120 min UV–O, the total oxygen content of the surface is 28.0 ± 0.3%, with COR, $R_2C{=}O$, and $RO{-}C{=}O$ binding proportions of 15.1 ± 0.9%, 10.6 ± 0.9%, and 2.3 ± 0.8%, respectively. The data indicate that overall, UV–O induced surface modification results in minimal changes in COR bonds (12.5–15.1%), doubling of $R_2C{=}O$ bonds (4.9–10.6%), and halving of $RO{-}C{=}O$ bonds (4.6–2.3%).

2.2.3. Overall Trends in Surface Chemistry

Attenuated total reflection Fourier transform infrared (ATR-FTIR) analysis of the UV–O treated pollen was performed to obtain a

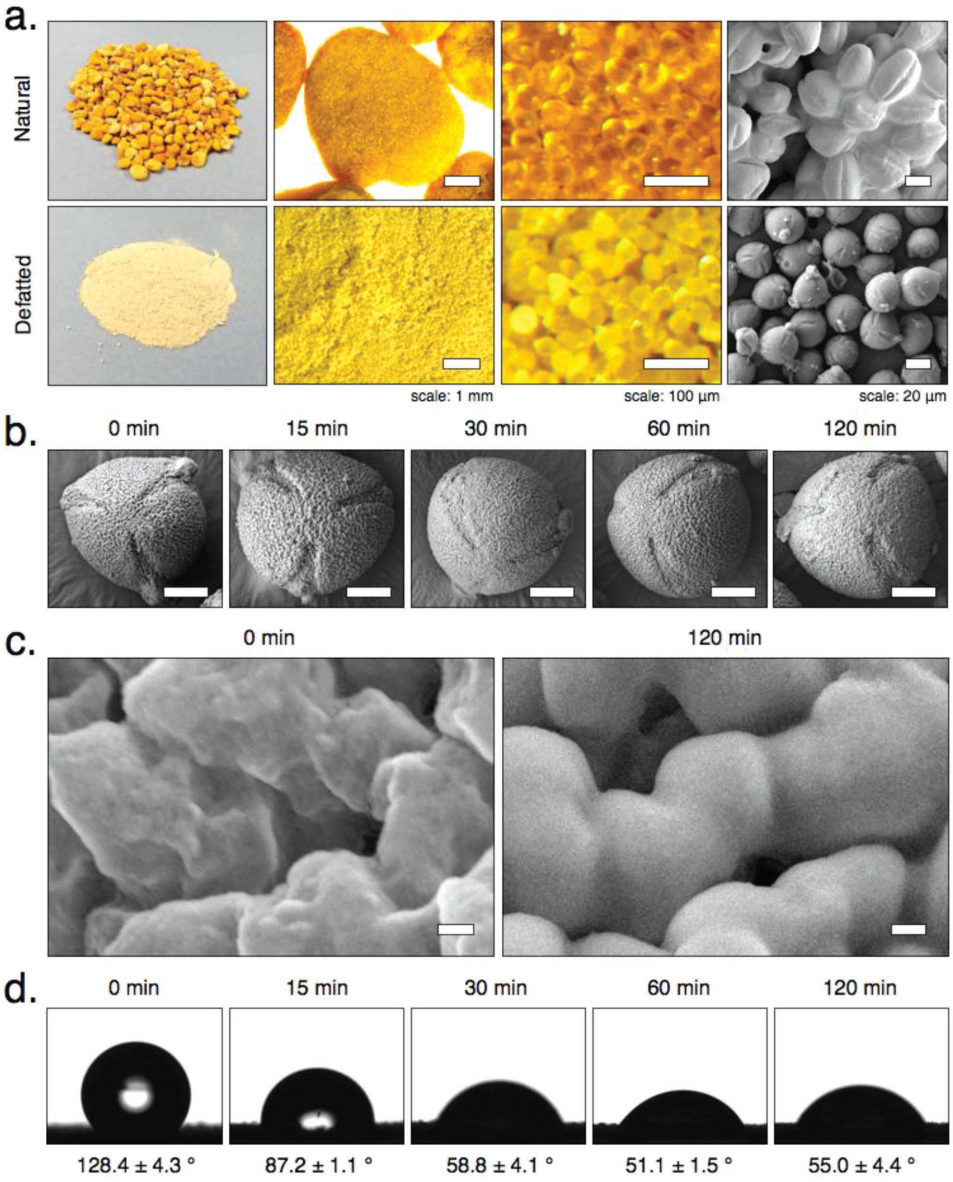

Figure 2. Defatted pollen extraction and ultraviolet–ozone (UV–O) treatment: a) photographs, stereo-micrographs, and scanning electron micrographs (SEM) of bee pollen granules and defatted pollen particles; b) SEM images of untreated and UV–O treated pollen particles; c) SEM images of untreated and UV–O treated pollen surfaces; and d) optical images of water droplet formation during contact measurements of untreated and UV–O treated pollen. Scale bars: (b) = 10 µm; (c) = 100 nm.

more complete understanding of surface chemistry changes, and provided verification of the observations made from X-ray photoelectron spectroscopy (XPS) analysis. Major peaks in untreated (0 min) pollen were assigned from previous FTIR studies on sporopollenin, with peak attributions being hydroxyl (3300 cm^{-1}), aliphatic (2925 cm^{-1}), carbonyl (1670 cm^{-1}) aromatics (1515 cm^{-1}, 1425 cm^{-1}), and COR (1028 cm^{-1}) (**Figure 4**a and Figure S7a, Supporting Information).[55,65] Subtracting UV–O treated spectra from untreated spectra suggested reductions in absorption for most major peaks of interest, and highlighted a relatively large increase in the shoulder peak at 1718 cm^{-1} (Figure 4b), which may be attributed to C=O[52] and correlates to the increased R_2C=O binding observed from the XPS analysis.

Peak height ratio analysis was performed on major peaks of interest and indicated that the broad strong 1028 cm^{-1} peak may be utilized as a relatively stable reference peak. All major peaks decrease or remain stable relative to the 1028 cm^{-1} peak as UV–O treatment duration is increased. Broad strong peaks in the 1300–900 cm^{-1} region can be typically attributed to COR bonds.[66,67] The XPS analysis data indicate that COR surface bonds are stable, and surface COR bonds may be attributed to the presence of ether or ester linkages in sporopollenin.[64,65,68] However, ATR-FTIR analysis penetrates the sample surface from 0.5 to 5+ µm depending on wavelength and angle of incidence,[69] and this can be expected to penetrate through the entire sporopollenin outer shell to the cellulosic

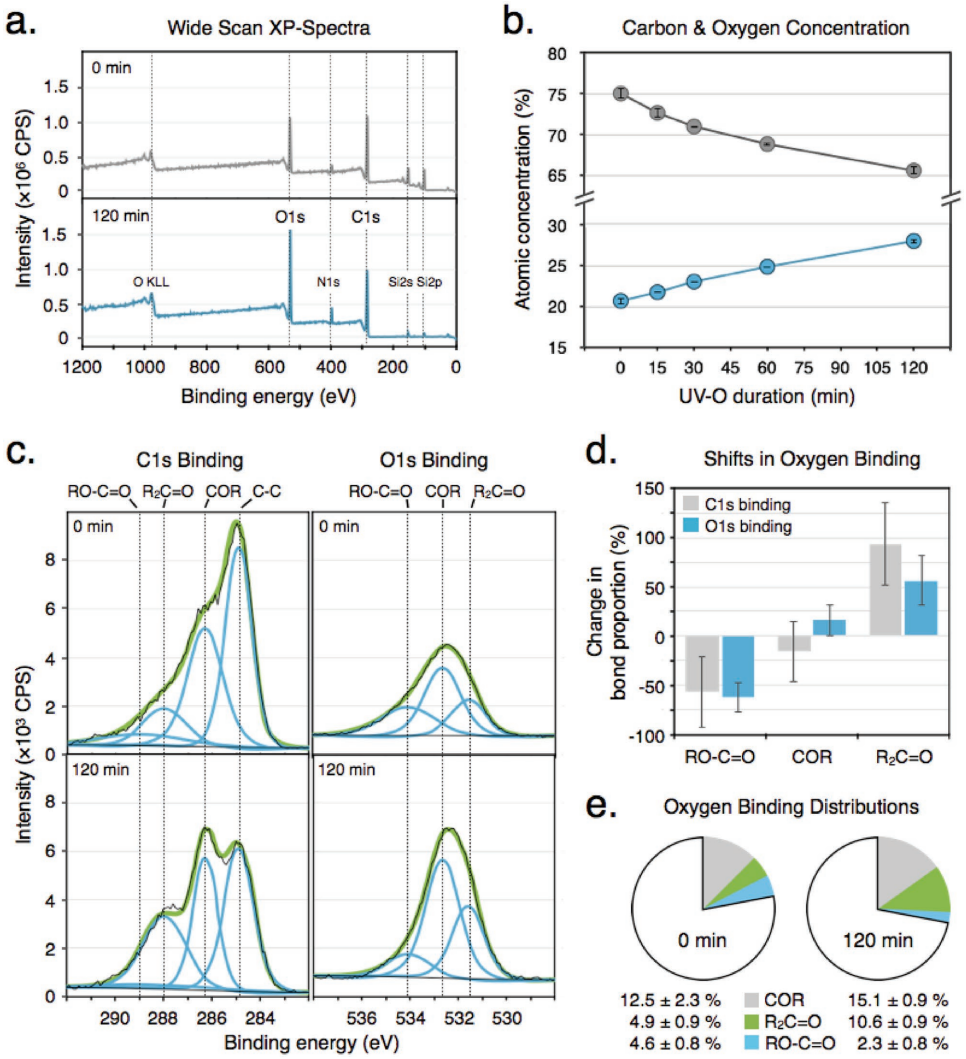

Figure 3. XPS analysis of untreated and ultraviolet–ozone (UV–O) treated pollen: a) wide-scan XP-spectra of untreated and 120 min UV–O treated pollen; b) carbon and oxygen elemental concentration of untreated and UV–O treated pollen; c) peak-fitting for chemical binding of carbon (C1s) and oxygen (O1s) peaks for untreated and 120 min UV–O treated pollen (black lines: raw data; blues lines: fitted peaks; green lines: fitted data); d) shifts in oxygen binding proportions with 120 min UV–O treatment; and e) total oxygen binding distributions for untreated and 120 min UV–O treated pollen.

intine (total sporoderm thickness = 1.8 ± 0.2, sporopollenin outer shell layer = 1.2 ± 0.2, and cellulosic inner shell layer = 0.6 ± 0.3).[26] In pollen, major FTIR peaks around 1028 cm^{-1} have also been shown to relate to COR binding in cellulosic compounds, which may be attributable to the inner sporoderm layer (intine).[69] Although the ATR-FTIR analysis will penetrate through the exine and intine to the pollen cytoplasm, both of the cytoplasmic internal genetic material and the cellulosic intine layer can be assumed to be protected by the robust sporopollenin exine layer and therefore resistant to modification by UV–O treatment. Therefore, due to the intine and cytoplasmic contents being protected from UV–O treatment, it is expected that the only variations in FTIR spectra will be due to surface modification of the sporopollenin. Overall, due to the stability

Table 1. Bond-type binding energies and proportions for carbon (C1s) and oxygen (O1s) binding.

Carbon (C1s)				Oxygen (O1s)			
Bond type	Binding energy [eV]	0 min [%]	120 min [%]	Bond type	Binding energy [eV]	0 min [%]	120 min [%]
CC/CH	284.9	43.0 ± 6.9	40.2 ± 6.6				
COR	286.3	37.3 ± 7.9	31.5 ± 3.6	COR	532.7	47.7 ± 7.2	55.5 ± 0.5
$R_2C=O$	288.0	13.3 ± 2.2	25.6 ± 3.4	$R_2C=O$	531.6	21.0 ± 4.5	32.8 ± 0.9
RO—C=O	289.0	6.1 ± 1.7	2.6 ± 0.5	RO—C=O	534.1	31.3 ± 4.1	11.7 ± 0.7

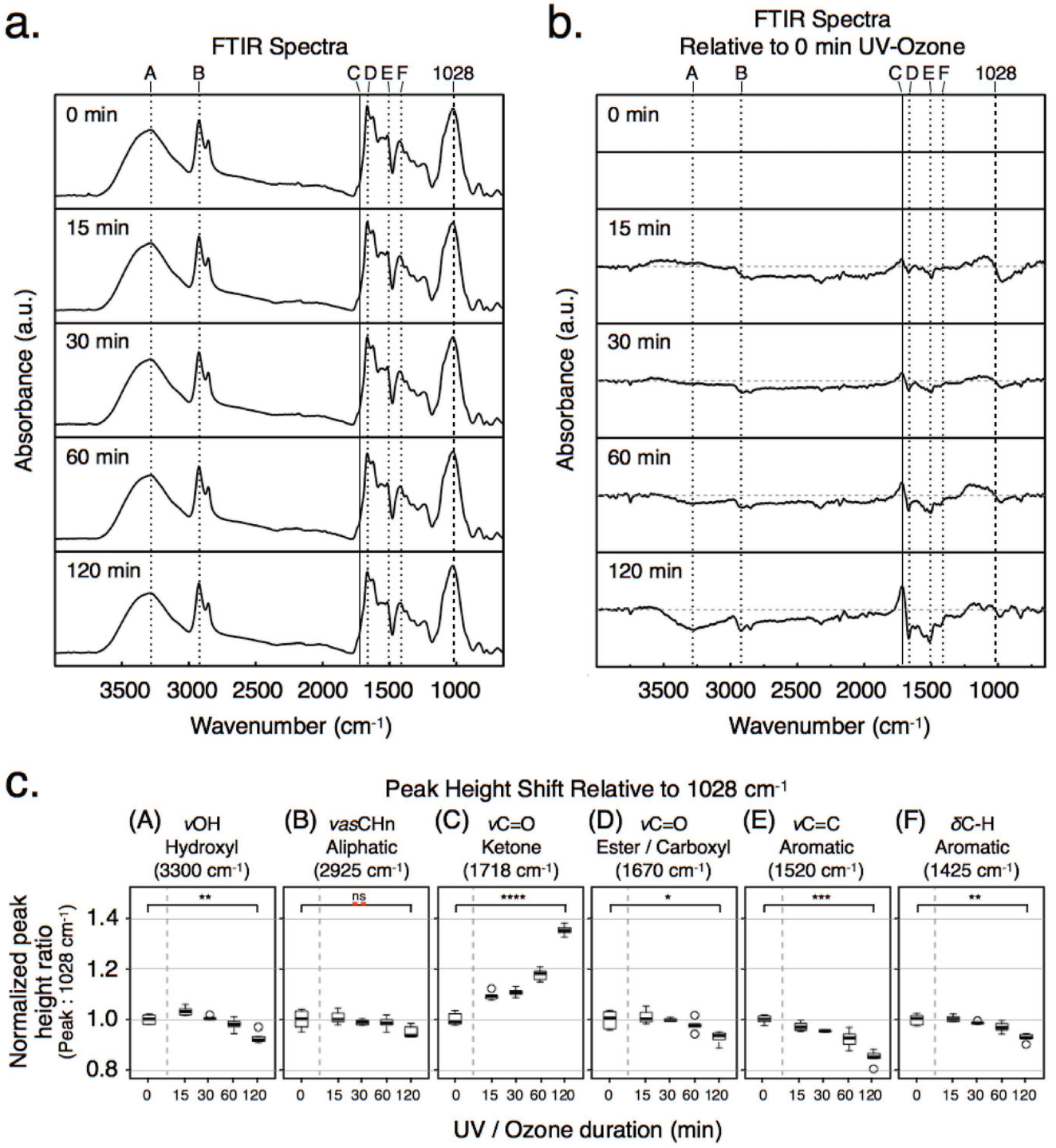

Figure 4. ATR-FTIR characterization of untreated and ultraviolet–ozone (UV–O) treated pollen: a) ATR-FTIR spectra of untreated and UV–O treated pollen; b) ATR-FTIR spectra of UV–O treated pollen relative to untreated pollen; and c) peak-height ratio analysis of untreated and UV–O treated pollen for major peaks of interest.

of the surface and intine COR bonds, subsequent peak height ratio analyses were performed relative to the 1028 cm^{-1} peak height.

Overall, peak height ratio analysis indicates that most bond types are reduced with increasing UV–O treatment, with the most significant reductions in aromatic ring νC=C bonds, and significant increases in νC=O bonds (Figure 4c and Figure S7b, Supporting Information). Normalized peak height ratio values from 120 min UV–O exposure for hydroxyl (νOH), aliphatic (*vas*CHn), ketone (νC=O), ester/carboxylic (νC=O), aromatic

(νC=C), and aromatic (dC−H) were 0.93 ± 0.02, 0.95 ± 0.02, 1.35 ± 0.02, 0.93 ± 0.02, 0.85 ± 0.03, and 0.93 ± 0.02, respectively. The decrease in absorbance of the aromatics may be attributed to UV–O treatment cleaving aromatic ring νC=C bonds[70,71] present in cinnamic acids in the sporopollenin biopolymer.[65] Studies from the ozonation of *p*-coumaric acid molecules, a primary constituent of sporopollenin, propose aromatic ring cleavage resulting in $R_2C{=}O$ groups attached to various remaining organic compound structures.[72] In sporopollenin, cinnamic acids act as crosslinking side-chains and are bound within the copolymer structure, therefore cleaving of aromatic rings within the cinnamic acids would be expected to produce an exposed $R_2C{=}O$ group attached within the copolymer, in a ketone formation. Correspondingly, our data indicate that the primary surface chemistry modification from UV–O treatment of pollen is the cleaving of aromatic rings resulting in the formation of $R_2C{=}O$ functional groups, which may be associated with ketone bonds.

It should be noted that the FTIR peak assignment of various carbonyl groups in sporopollenin is challenging due to variation, complexity, and uncertainty in sporopollenin chemistry. However, the XPS data from this study indicate an increase in $R_2C{=}O$ and a decrease RO−C=O, and the FTIR data indicate an increase in carbonyls at 1718 cm^{-1} and a decrease in carbonyls at 1670 cm^{-1}, therefore the data suggest that 1718 cm^{-1} (νC=O) may be attributed to ketones, and 1670 cm^{-1} (νC=O) may be attributed to either esters or carboxylic acids. Such information, correlated through multiple independent methods, provides an interpretative framework to understand the spectral responses of different functional groups present in sporopollenin and these insights complement other recent studies as well.[46,55]

2.3. Applications of UV–Ozone Surface Modified Pollen

2.3.1. Aqueous Suspensions and Pickering Emulsions

UV–O treatment of pollen reduced particle clustering in water and allowed for tuning of Pickering emulsion properties. Decreasing particle hydrophobicity reduced the proportion of large clusters of particles, with the number of 90+ µm clusters being significantly ($p < 0.01$) reduced after 120 min UV–O. Overall, after 120 min UV–O, the relative proportion of 30–50 µm, 50–90 µm, 90–150 µm, and 150+ µm particle clusters was 1.22 ± 0.14, 0.88 ± 0.15, 0.47 ± 0.15, and 0.10 ± 0.04, respectively (**Figure 5**a and Figure S8, Supporting Information), with cluster sizes representing particle counts of ≈1, 2–6, 7–20, and 21+ particles (Figure 5b and Figure S9, Supporting Information). The reduction in particle clustering, for clusters greater than six particles, may be attributed to improved particle wetting and thus improved affinity to water.

Analysis of oil and water systems stabilized by untreated and UV–O treated pollen indicated that pollen can be used to form microparticle stabilized Pickering emulsions, and that UV–O treatment allowed for tuning of emulsion properties. Emulsions were formed with isopropyl myristate as the oil phase and deionized (DI) water as the aqueous phase, along with 0, 15, and 120 min UV–O treated pollen, and were allowed to stabilize for one week (Figure S10, Supporting Information). Overall, emulsions formed with 0, 15, and 120 min UV–O treated pollen resulted in oil fractions (f_{oil}) of 0.33 ± 0.05, 0.11 ± 0.03, and 0.51 ± 0.08, and aqueous fractions (f_{aq}) of 0.94 ± 0.05, 0.92 ± 0.01, and 0.79 ± 0.08, respectively (Figure 5c). The addition of a lipophilic dye (Nile red) to the emulsions indicated that all emulsions comprised oil droplets in an aqueous continuous phase (o/w) (Figure S11, Supporting Information).

The degree of UV–O treatment influences the pollen particle to oil droplet interaction dynamics. Prolonged UV–O treatment duration appeared to reduce the number of pollen particles per unit area adhering to the oil droplets (Figure 5d and Figure S11, Supporting Information). Further, confocal laser scanning microscopy (CLSM) imaging of emulsion samples indicated that for both 0 and 120 min samples, excess pollen particles settled to the bottom of the sample, whereas with the 15 min sample there were few settled particles (Figure 5e and Figure S12, Supporting Information). For the 0 min sample, the settled pollen is typically bound to the oil phase on the glass slide surface, suggesting that the untreated pollen has strong affinity to the oil and that as excess pollen particles settle they draw oil to the bottom of the emulsion. For the 15 and 120 min samples there is no observed pollen/oil binding on the glass slide surface, suggesting that these systems may be more stable. The 15 min sample results in minimal excess settled particles, indicating an appropriate oil to particle ratio. Whereas, the 120 min sample has numerous excess settled particles, indicating that it may be possible to reduce the proportion of particles necessary to stabilize the emulsion.

Overall, both untreated and UV–O treated pollens were able to form Pickering emulsions with varying properties, with reductions in oil droplet size (Figure 5f). Untreated (0 min) pollen formed emulsions with a yield of 36.4 ± 5.4% of initial oil + water, comprising ≈92% oil and ≈8% water, resulting in an oil:water proportion of 11.0:1, and oil droplets of ≈1.0–3.0 mm diameter. Pollen treated for 15 min produced emulsions with an increased overall yield of 48.8 ± 11.1% of initial oil + water, comprising ≈91% oil and ≈9% water, resulting in an oil:water proportion of 10.5:1, and oil droplets of ≈0.6–1.3 mm diameter. Whereas, pollen treated for 120 min produced emulsions with an overall yield of 34.7 ± 4.9% of initial oil + water, but with an increased proportion of water, comprising ≈70% oil and ≈30% water, resulting in an oil:water proportion of 2.4:1, and oil droplets of ≈0.2–0.8 mm diameter. Therefore, both untreated and UV–O treated pollens are effective in stabilizing emulsions, and may be utilized depending on the desired application. It should also be noted that prolonged UV–O treatment of pollen facilitates greater water uptake into the emulsion.

2.3.2. Pollen/Cell Binding Enhancement

UV–O treatment of pollen enhanced cell binding to pollen grains, indicating that it is possible to tune cell-pollen affinity and interactions. Cells (Huh-7.5, liver hepatocytes) were seeded and incubated for 24 h to ensure a stable sub-layer for pollen adhesion. Pollen grains were added, and the pollen/cell system was incubated for a further 24 h to determine whether cells would adhere to untreated and/or UV–O treated pollen while

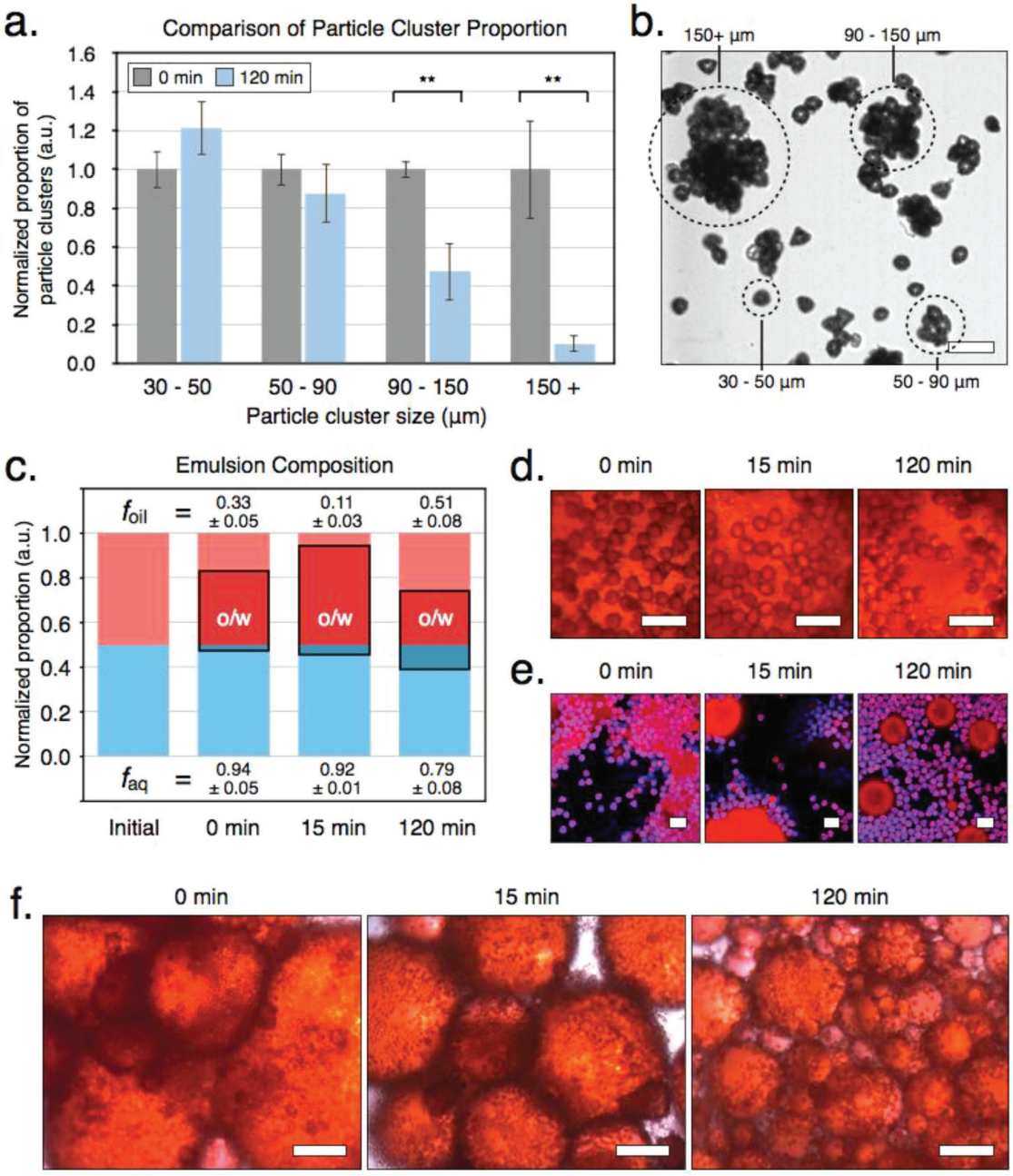

Figure 5. Aqueous suspension and Pickering emulsion properties of untreated and ultraviolet–ozone (UV–O) treated pollen: a) comparison of pollen particle cluster proportions for untreated and 120 min UV–O treated pollen; b) optical microscope image depicting examples of cluster size; c) diagrammatic depiction of emulsion composition, for untreated and UV–O treated pollen; d) stereo-microscope images of pollen particles on Nile red stained oil droplets in emulsions comprising untreated and UV–O treated pollen; e) confocal laser scanning microscopy (CLSM) images of pollen particle stabilized Pickering emulsions incorporating a hydrophobic dye, Nile red, with untreated and UV–O treated pollen particles; and f) stereo-microscope images of pollen particle stabilized Pickering emulsions incorporating a hydrophobic dye, Nile red, with untreated and UV–O treated pollen particles. Scale bars: (b), (d), and (e) = 100 µm; (f) = 500 µm.

sitting atop them. Both untreated and UV–O treated pollen resulted in some proportion of pollen becoming adhered to the stable cell sub-layer. During washing to quantify pollen binding, live microscopy imaging indicated that poorly-bound pollen were removed while well-bound pollen remained attached (**Figure 6**a and Video S1, Supporting Information). Quantification of the removed pollen by DIPA indicated that the proportion of bound pollen increased with UV–O treatment, with 120 min UV–O resulting in 2.6 ± 0.2 times more pollen being bound (Figure 6b). CLSM analysis suggests that cells incubated with UV–O treated pollen had a greater tendency to proliferate around the base of the pollen (Figure 6c and Figures S13 and S14 and Video S2, Supporting Information). Cells are depicted in green due to immunostaining, whereas pollens are

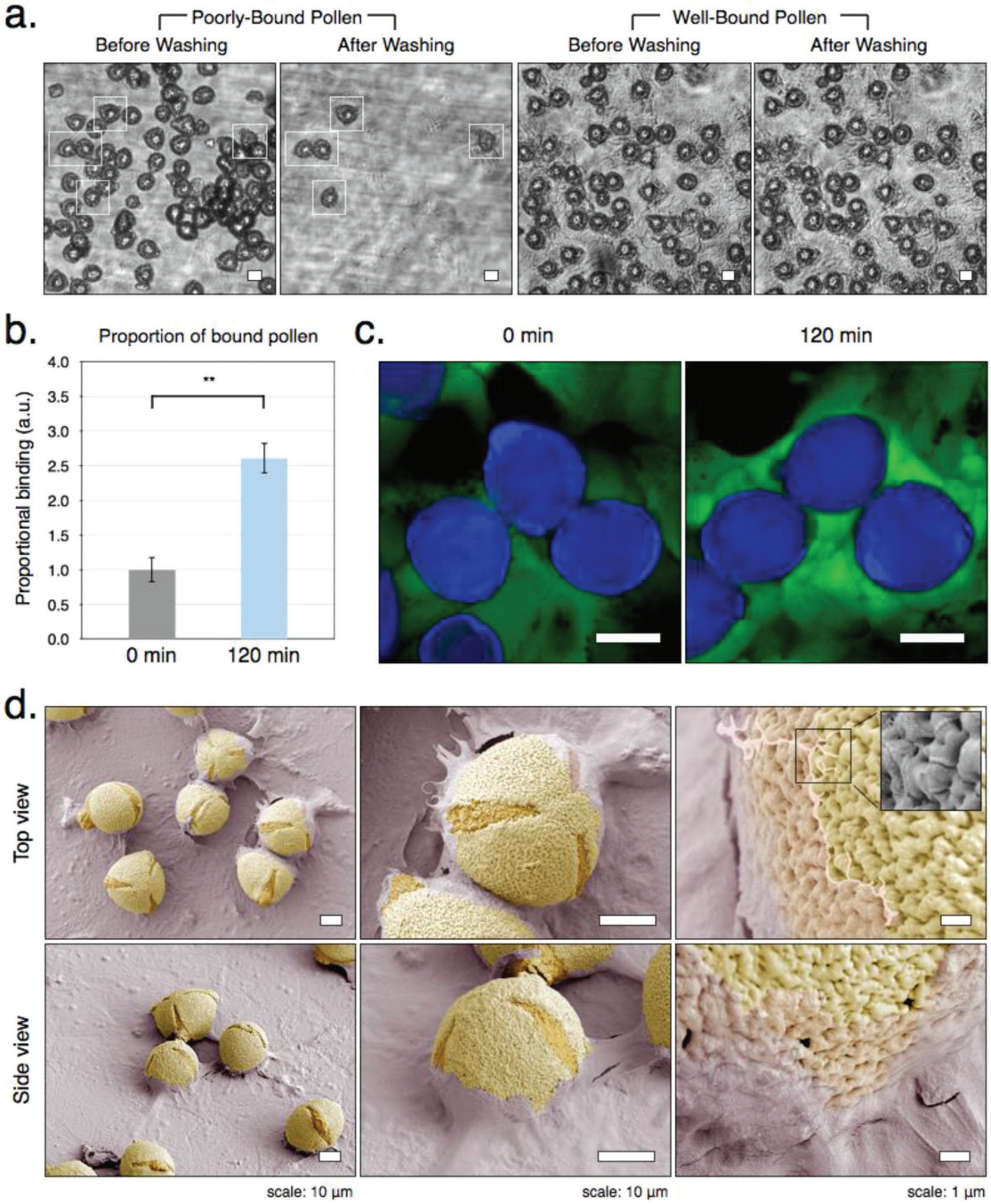

Figure 6. Pollen/cell binding properties for untreated and ultraviolet–ozone (UV–O) treated pollen binding with Huh-7.5 liver hepatocytes: a) optical micrographs of pollen/cell binding for poorly-bound pollen and well-bound pollen before and after washing; b) relative pollen binding for untreated and UV–O treated pollen showing data for multiple measurements of multiple batches; c) confocal laser scanning microscopy (CLSM) 3D z-stack reconstructions for untreated and UV–O treated pollen; and d) false-color scanning electron microscopy (SEM) images of pollen/cell binding for well-bound UV–O treated pollen (original uncolored images can be found in Figure S11, Supporting Information). Scale bars: (a) and (c) = 20 µm.

shown in blue due to autofluorescence. Samples were analyzed with CLSM while still in cell-culture media and without any washing to remove unbound pollen. Typically, there are more bright green regions surrounding the pollen particles when the pollen has been UV–O treated, which may be attributed to a thicker layer of cells surrounding the base of well-bound pollen. Analysis of CLSM z-stack slices indicates that cells typically formed a 5–10 µm base layer of cells, but grew to a total height of 15–20 µm when surrounding UV–O treated pollen particles (Figure S14, Supporting Information). Imaging with SEM provides direct observations of cell proliferation and attachment around the base of well-bound pollen. Cell growth can be seen

up to the lower third of the pollen (≈12 µm), and cells appear to adhere to the pollen surface (Figure 6d and Figure S15, Supporting Information). Fibrils originating from the cells were observed on the surface of pollen at the boundary of the cell coverage, suggesting that the process of cell attachment to pollen is led by the spreading of actin filopodia filaments.[73]

These results highlight that $R_2C{=}O$ ketone functionalities may play a key role in enhanced cell adhesion from UV–O surface modification of aromatic polymers, such as polystyrene. Studies on UV–O functionalization of polystyrene for enhanced cell culture suggest that cell growth enhancement may be attributed to additional OH, COR, RO−C=O, and $R_2C{=}O$ groups,[50,74,75] with particular importance given to ester/carboxylic acid functionalities (RO−C=O).[74] However, as discussed above, our studies indicate that for aromatic ring opening of sporopollenin, the only increases in functional group type are seen for $R_2C{=}O$ ketone bonds, supporting that ketone-mediated changes in surface hydrophilicity can also promote enhanced adhesion.

Overall, enhancement of pollen/cell adhesion suggests that UV–O treatment of pollen produces functional microparticles that are suitable for use in internal and topical applications, and may be better suited to drug/compound delivery applications. Although, UV–O has been shown to enhance polymer/cell adhesion to other cell types, such as, stem cells,[50,74] and ovarian cells,[75] the use of hepatocarcinoma cells in this study suggests potential benefits to developing topical formulations for treating various cancers, such as basal-cell skin cancer, squamous-cell skin cancer, and melanoma.

3. Conclusion

Surface modification of pollen derived from bee-collected *C. sinensis* pollen granules may be utilized to control surface chemistry, enhance wetting and dispersion properties, tune Pickering emulsion properties, and improve pollen/cell adhesion. High purity, monodisperse pollen particles may be obtained from bee-collected pollen granules through washing and defatting. Pollen particles are known to be amphiphilic though typically more hydrophobic; however, UV–O treatment results in enhanced surface wetting. The resulting degradation leads to altered pollen surface chemistry, increasing the proportion of surface oxygen with significant increases in $R_2C{=}O$ ketone binding, yet reducing the proportions of most other chemical bonds, with the most significant reductions in C=C binding. Decreases in C=C binding with concomitant increases in $R_2C{=}O$ binding may be attributed to opening of aromatic ring structures present in the pollen shell biopolymer, with the formation of new $R_2C{=}O$ ketone bonds.

Control over pollen surface chemistry provides a means for enhancing the utility of pollen in a wide range of applications. The enhancement of surface wetting from increased $R_2C{=}O$ ketone binding correlates with improved dispersion properties by reducing particle clustering. Further, UV–O treatment of pollen is shown to modify the properties of microparticle stabilized Pickering emulsions, leading to shifts in emulsion stability, emulsion yields, proportions of oil-to-water, proportions of pollen particles required, and oil droplet size. The ability to tune emulsion properties through the simple process of UV–O treatment expands the potential applications for utilizing pollen in natural consumer products. Finally, UV–O treatment is shown to enhance the binding affinity of pollen and liver hepatocarcinoma cells. Pollen particles are known to be biocompatible; however, this is the first study to highlight and enhance pollen/cell binding affinities, and an awareness of pollen/cell binding has potential implications for a wide range of fields, from biology and pollination, to natural product development and drug delivery.

Looking forward, pollen particles offer an attractive material for developing natural oil/water based products for natural foods, cosmetics, and herbal therapeutics. Herein, we have highlighted the potential of surface modification through UV–O treatment to tune the interfacial properties of pollen and thereby exhibit greater control over system properties. These observations open the way for ongoing fundamental and applied research in this field, and expand the potential of pollen as an important source of regulation-free natural functional microparticles.

4. Experimental Section

Materials: C. sinensis bee pollen granules were purchased from Xi'an Yuensun Biological Technology Company Limited (China). Acetone was obtained from Aik Moh Paints & Chemicals Pte Ltd (Singapore). Diethyl ether and absolute ethanol were procured from Merck Millipore Corporation (USA). Isopropyl myristate, sodium chloride, Nile red, and glutaraldehyde solution were purchased from Sigma-Aldrich Pte Ltd (USA). Nylon mesh was purchased from ELKO Filtering Co. LLC (USA). Duke polystyrene microsphere standards (50 ± 1 µm), Dulbecco's Modified Eagle Medium (DMEM), fetal bovine serum (10%), penicillin-streptomycin (1%), LIVE/DEAD Viability/Cytotoxicity Kit, for mammalian cells and flat bottom Nunclon Delta 24-well plates were purchased from Thermo Scientific Pte Ltd (USA). Human hepatocellular carcinoma cells (Huh-7.5) were purchased from Apath (USA).

Defatting of Bee Pollen Granules: C. sinensis bee pollen granules (250 g) were suspended in acetone (500 mL) and refluxed in a round bottom flask (50 °C, 220 rpm, 3 h). After that, acetone was decanted and DI water (1000 mL, 50 °C) was added to the sample, mixed, and bath-sonicated (10 min). The sample and water mixture was passed through nylon mesh (150 µm) to remove contaminant particulate matter. Water was removed from resulting filtrate using vacuum filtration. Next, the sample was mixed with DI water (1000 mL, 50 °C) and filtered. The resulting sample was suspended in acetone (500 mL) and refluxed (50 °C, 220 rpm, 3 h). After that acetone was removed and defatted pollen was transferred to a petri dish and left to dry in a fume hood (12 h). After defatting with acetone, dry sample (20 g) was mixed with diethyl ether (250 mL) with stirring (25 °C, 300 rpm, 2 h). Diethyl ether defatting was done twice and each time fresh diethyl ether was used. Removal of diethyl ether was done by vacuum filtration. After washing with diethyl ether twice, the sample was added to fresh diethyl ether and left to stir overnight (25 °C, 300 rpm, 12 h). Diethyl ether was removed and the sample was transferred to a petri dish and left to dry in a fume hood (12 h).

UV–O Treatment: UV–O treatment was carried out on pollen grains (50 mg) for various durations (15, 30, 60, and 120 min). Pollen grains were spread evenly on a plastic disposable petri dish (90 × 15 mm) and exposed to UV–O (12188 W m^{-1}) using a benchtop PSD Series UV–O cleaner (Novascan, USA).

Contact Angle Measurements: Contact angle measurements were performed with pollen particles (0, 15, 30, 60, and 120 min UV–O). A thin layer or pollen was spread on self-adhesive carbon tape (5 mm × 5 mm) on a glass slide and a bead of DI water (2 µL) was slowly lowered onto the layer of pollen. The contact angle was measured using

an Attension Theta Optical Tensiometer (Biolin Scientific Holding AB, Sweden) (0.7 X magnification, 20 s, 12 frames per second (FPS)) with OneAttension 1.0 software.

X-Ray Photoelectron Spectroscopy: Wide (160 eV) scan XPS was performed with pollen particles (0, 15, 30, 60, and 120 min UV–O), and narrow (20 eV) scan XPS was performed with pollen particles (0 and 120 min UV–O). Pollen particles were dried using a freeze drier overnight (12 h) before UV–O treatment. Pollen particles were deposited on carbon tape (5 mm × 5 mm) adhered to a silicon wafer. Samples were analyzed using AXIS Supra (XPS) surface analysis instrument (Kratos Analytical Ltd, UK) equipped with a monochromatic Al/Mg X-ray source (225 W, 2×10^{-9} mbar). Spectra were obtained using an aluminum anode (Al Kα = 1491.600 eV) and charge neutralization.

Attenuated Total Reflection Fourier Transform Infrared Spectroscopy: ATR-FTIR analysis was performed with pollen particles exposed to UV–O (0, 15, 30, 60, and 120 min). Absorbance spectra were obtained using a Perkin Elmer Frontier FTIR spectrometer with a universal ATR sampling accessory. A layer of sample was placed on the diamond/ZnSe crystal of the FTIR ATR accessory and the sample holder was lowered gently onto sample to ensure good contact with the crystal. Samples were scanned (from 4000 to 600 cm^{-1}, with 16 scan accumulations, at resolution of 32 cm^{-1} and data interval of 1 cm^{-1}), backgrounded, baselined, and smoothed using Spectrum v10.5 program. Six separate sets of ATR-FTIR data were collected for each sample. Data gathered were normalized to a standard peak (1028 cm^{-1}) and plotted in Origin. Peak heights of specific functional groups were extracted and ratios between functional group peak heights were calculated.

Dynamic Image Particle Analysis: Dynamic image particle analysis was performed as described elsewhere.[26] Briefly, the system was setup with a flow cell (200 µm) and a lens (4x). For particle clustering analysis, pollen particle (0 and 120 min) solutions were prepared (2 mg mL^{-1}) and added to the flow cell at a constant flow rate. For particle/cell adhesion quantification, water (2 mL) was added to the extracted pollen and vortexed (10 s), and then the solution was added to the flow cell at a constant flow rate.

Pickering Emulsions: Pickering emulsions were made using pollen grains (0, 15, and 120 min UV–O). Suspensions of pollen particles (250 mg) in isopropyl myristate (5 mL) were made using a probe sonicator (probe tip diameter of 30 mm, 20 kHz, 10 W, 2 min), then added to a glass vial (20 mL) containing sodium chloride solution (10×10^{-3} M, 5 mL). Water phase, oil phase, and particle system were then agitated using an IKA Ultra Turrax T18 rotorstator mixer (IKA Works GmbH & Co. KG, Germany) (1.0 cm dispersing head, 19 000 rpm, 2 min). For imaging purposes to differentiate between oil and water, the oil phase was dyed with Nile red (0.3 mg mL^{-1}). Heights of the emulsion, oil, and water layer were recorded initially and after one week.

Pollen/Cell Adhesion Study: Human hepatocellular carcinoma cells, Huh-7.5 cells were used in this study. Culture media used was made of DMEM (1x), fetal bovine serum (10%), and penicillin-streptomycin (1%). For sterilization, each type of pollen particles (30 mg) was incubated in diethyl ether overnight and dried with the aid of a vacuum oven (25 °C, 100 mbar) till stable weight. Pollen samples used in this study were 0 min UV–O and 120 min UV–O *C. sinensis* pollen. Cells were seeded (seeding concentration of 100 000 cells per well) onto the 24-well tissue culture plates with culture media (1 mL). Cells were incubated (24 h) to allow for attachment to the culture plate. After 24 h, the culture media was replaced with fresh culture media containing 50 000 pollen particles (1.6 mg of pollen) and left to incubate (24 h). After incubation, media was collected from the wells and each well was washed with culture media (1 mL) two times. All supernatants were collected and the solution was centrifuged (5000 × g, 25 °C, 5 min) to collect the unbound pollen particles. Collected pollen particles were quantified by DIPA and the number of attached particles was calculated.

CLSM Analysis: CLSM was performed as described elsewhere.[26] Briefly, samples were imaged in a 24-well plate. Imaging was performed successively with three laser excitation channels: 405, 488, and 561 nm, with three respective emission filters: 416–477, 498–550, and 572–620 nm. A regular objective lens (20 ×) was used for imaging. At least three images were captured per sample. Z-stack slices were taken (Z-stack thickness of 4 µm, 2 µm interval, bidirectional laser scanning, scan speed of 6, pixel averaging of 2, 12 slices) and reconstructed using ZEN and 3D images were obtained. For cell studies, calcein acetoxymethyl in culture media (1 µL mL^{-1}) was added to samples and allowed to incubate (1 h, 37 °C, 5% CO_2).

Bright Field Microscopy: Bright field microscopy was performed with samples prepared from the pollen/cell adhesion study protocol. Images and videos were obtained using Nikon Eclipse Ti-E Inverted Microscope System (Nikon Instruments Inc., USA) linked up with NIS-Elements AR Microscope Imaging Software Version 4.0 (Nikon Instruments Inc., USA). A 24-well plate was placed on microscope stage and a micropipette was used to agitate the pollen particles. Videos of unbound pollen particles being washed away in the 24-well plate were recorded (5 FPS for 1 min). Images were extracted from videos using ImageJ.

Surface Morphology Evaluation by Scanning Electron Microscopy: SEM imaging was performed with a JSM 7600F (JEOL, Japan) system. Briefly, samples were coated with gold using an auto fine coater JFC-1600 (JEOL, Japan) (20 mA, 80 s, distance from target is 3 cm) and images were obtained with an acceleration voltage of 5.00 kV at various magnifications. For cell studies, cells were fixed with glutaraldehyde (4%, 40 min), washed three times with PBS (5 min), followed by sequential ethanol dehydration (EtOH 25%, 50%, 75%, 95%, 100% for 20 min each), freezing (–80 °C, 12 h), and freeze-drying (24 h).

Evaluation of Pickering Emulsion by Stereomicroscopy: Stereomicroscope imaging was performed on Pickering emulsion droplets using a Nikon SMZ1000 Zoom Stereomicroscope (Nikon Instruments Inc., USA) equipped with an LV-TV adapter connected to a digital camera and linked to NIS-Elements F Microscope Imaging Software Version 4.0 (Nikon Instruments Inc., USA). A dropper was used to transfer emulsion samples (≈200 µL) onto a glass slide and images were taken at various magnifications.

Statistical Analysis: Statistical analysis of data was performed based on two-tailed *t*-tests, with $P < 0.05$ being statistically significant. Quantitative data from DIPA, contact angle measurements, and XPS were collected in triplicate and the results are expressed as mean ± standard deviation (SD) of the mean.

Supporting Information

Supporting Information is available from the Wiley Online Library or from the author.

Acknowledgements

This research was supported by the Creative Materials Discovery Program through the National Research Foundation of Korea (NRF) funded by the Ministry of Science, ICT, and Future Planning (NRF-2016M3D1A1024098). This work was also supported by the Competitive Research Programme (NRF-CRP10-2012-07) of the National Research Foundation of Singapore (NRF). The research was also supported by a Start-Up Grant (SUG) from Nanyang Technological University (M4080751.070). Many thanks are due to Dr. S. Meker for her input regarding the interpretation of surface chemistry modification data; to Dr. Y. N. Liang from the Nanyang Environment & Water Research Institute (NEWRI) for collection of the XPS data; to Dr. S. Pedersen for his assistance with utilizing R-Code for data analysis; and to Ekaterina (Katya) Stonkevitch for her diligent efforts aiding in sample preparation and data collection.

Conflict of Interest

The authors declare no conflict of interest.

Keywords

cellular adhesion, colloids, pollen microparticles, surface modification, ultraviolet–ozone treatment

Received: December 29, 2017
Revised: January 27, 2018
Published online: March 1, 2018

[1] C. C. Berton-Carabin, K. Schroën, *Annu. Rev. Food Sci. Technol.* **2015**, *6*, 263.
[2] C. Y. Tham, W. S. Chow, *Colloids Surf., A* **2017**, *533*, 275.
[3] C. Chang, F. Niu, L. Gu, X. Li, H. Yang, B. Zhou, J. Wang, Y. Su, Y. Yang, *Food Hydrocolloids* **2016**, *61*, 477.
[4] M. Ago, S. Huan, M. Borghei, J. Raula, E. I. Kauppinen, O. J. Rojas, *ACS Appl. Mater. Interfaces* **2016**, *8*, 23302.
[5] Y. Hu, X. Gu, Y. Yang, J. Huang, M. Hu, W. Chen, Z. Tong, C. Wang, *ACS Appl. Mater. Interfaces* **2014**, *6*, 17166.
[6] J. Dong, A. J. Worthen, L. M. Foster, Y. Chen, K. A. Cornell, S. L. Bryant, T. M. Truskett, C. W. Bielawski, K. P. Johnston, *ACS Appl. Mater. Interfaces* **2014**, *6*, 11502.
[7] M. l. Marquis, V. Alix, I. Capron, S. p. Cuenot, A. Zykwinska, *ACS Biomater. Sci. Eng.* **2016**, *2*, 535.
[8] E. Dickinson, *Food Hydrocolloids* **2017**, *68*, 219.
[9] L. Wei, M. Zhang, X. Zhang, H. Xin, H. Yang, *ACS Sustainable Chem. Eng.* **2016**, *4*, 6838.
[10] J. Marto, A. Ascenso, S. Simoes, A. J. Almeida, H. M. Ribeiro, *Expert Opin. Drug Delivery* **2016**, *13*, 1093.
[11] J. Xiao, Y. Li, Q. Huang, *Trends Food Sci. Technol.* **2016**, *55*, 48.
[12] B. P. Binks, *Langmuir* **2017**, *33*, 6947.
[13] M. G. Potroz, R. C. Mundargi, J. J. Gillissen, E. L. Tan, S. Meker, J. H. Park, H. Jung, S. Park, D. Cho, S. I. Bang, *Adv. Funct. Mater.* **2017**, *27*, 1700270.
[14] W. Montgomery, C. Potiszil, J. S. Watson, M. A. Sephton, *Macromol. Chem. Phys.* **2016**, *217*, 2494.
[15] H. Lin, L. Lizarraga, L. A. Bottomley, J. C. Meredith, *J. Colloid Interface. Sci.* **2015**, *442*, 133.
[16] H. Linskens, W. Jorde, *Econ. Bot.* **1997**, *51*, 78.
[17] S. P. de Souza, J. Bassut, H. V. Marquez, I. I. Junior, L. S. Miranda, Y. Huang, G. Mackenzie, A. N. Boa, R. O. de Souza, *Catal. Sci. Technol.* **2015**, *5*, 3130.
[18] S. Barrier, A. Löbbert, A. J. Boasman, A. N. Boa, M. Lorch, S. L. Atkin, G. Mackenzie, *Green Chem.* **2010**, *12*, 234.
[19] G. Mackenzie, A. N. Boa, A. Diego-Taboada, S. L. Atkin, T. Sathyapalan, *Front. Mater.* **2015**, *2*, 66.
[20] C. Chiappe, G. C. Demontis, V. Di Bussolo, M. J. R. Douton, F. Rossella, C. S. Pomelli, S. Sartini, S. Caporali, *Green Chem.* **2017**, *19*, 1028.
[21] L. R. Johnstone, I. J. Gomez, H. Lin, O. O. Fadiran, V. W. Chen, J. C. Meredith, J. W. Perry, *ACS Appl. Mater. Interfaces* **2017**, *9*, 24804.
[22] H. Lin, M. C. Allen, J. Wu, B. M. deGlee, D. Shin, Y. Cai, K. H. Sandhage, D. D. Deheyn, J. C. Meredith, *Chem. Mater.* **2015**, *27*, 7321.
[23] W. B. Goodwin, D. Shin, D. Sabo, S. Hwang, Z. J. Zhang, J. C. Meredith, K. H. Sandhage, *Bioinspiration Biomimetics* **2017**, *12*, 066009.
[24] S. U. Atwe, Y. Ma, H. S. Gill, *J. Controlled Release* **2014**, *194*, 45.
[25] M. G. Potroz, R. C. Mundargi, J. H. Park, E.-L. Tan, N.-j. Cho, *JoVE* **2016**, *117*, e54768.
[26] R. C. Mundargi, M. G. Potroz, J. H. Park, J. Seo, E. L. Tan, J. H. Lee, N. J. Cho, *Sci. Rep.* **2016**, *6*, 19960.
[27] R. C. Mundargi, M. G. Potroz, J. H. Park, J. Seo, J. H. Lee, N.-J. Cho, *RSC Adv.* **2016**, *6*, 16533.
[28] A. K. Prabhakar, H. Y. Lai, M. G. Potroz, M. K. Corliss, J. H. Park, R. C. Mundargi, D. Cho, S.-I. Bang, N.-J. Cho, *Ind. Eng. Chem. Res.* **2017**, *53*, 375.
[29] I. Sargin, L. Akyuz, M. Kaya, G. Tan, T. Ceter, K. Yildirim, S. Ertosun, G. H. Aydin, M. Topal, *Int. J. Biol. Macromol.* **2017**, *105*, 749.
[30] A. Diego-Taboada, S. T. Beckett, S. L. Atkin, G. Mackenzie, *Pharmaceutics* **2014**, *6*, 80.
[31] T. Larkin, *FDA Consum.* **1984**, *18*, 21.
[32] L. Almeida-Muradian, L. C. Pamplona, S. l. Coimbra, O. M. Barth, *J. Food Compos. Anal.* **2005**, *18*, 105.
[33] B. P. Binks, J. Clint, G. Mackenzie, C. Simcock, C. Whitby, *Langmuir* **2005**, *21*, 8161.
[34] S. Barrier, A. Diego-Taboada, M. J. Thomasson, L. Madden, J. C. Pointon, J. D. Wadhawan, S. T. Beckett, S. L. Atkin, G. Mackenzie, *J. Mater. Chem.* **2011**, *21*, 975.
[35] W. Cai, *PhD Thesis*, University of York, **2014**.
[36] S. H. Buhner, *Pine Pollen: Ancient Medicine for a New Millennium*, BookBaby, Oregon, USA **2012**.
[37] L. Cornara, M. Biagi, J. Xiao, B. Burlando, *Front Pharmacol.* **2017**, *8*, 412.
[38] B. Denisow, M. Denisow-Pietrzyk, *J. Sci. Food Agric.* **2016**, *96*, 4303.
[39] R. C. Mundargi, M. G. Potroz, S. Park, H. Shirahama, J. H. Lee, J. Seo, N.-J. Cho, *Small* **2015**, *12*, 1167.
[40] R. C. Mundargi, M. G. Potroz, S. Park, J. H. Park, H. Shirahama, J. H. Lee, J. Seo, N. J. Cho, *Adv. Funct. Mater.* **2015**, *26*, 487.
[41] R. C. Mundargi, E.-L. Tan, J. Seo, N.-J. Cho, *Ind. Eng. Chem. Res.* **2016**, *36*, 102.
[42] W.-F. Lai, A. L. Rogach, *ACS Appl. Mater. Interfaces* **2017**, *9*, 11309.
[43] P. Prabhakar, A. Kumar, M. Doble, *Phytomedicine* **2014**, *21*, 123.
[44] K. Komosinska-Vassev, P. Olczyk, J. Kaźmierczak, L. Mencner, K. Olczyk, *J. Evidence-Based Complementary Altern. Med.* **2015**, *2015*, 297425.
[45] B. P. Binks, A. N. Boa, M. A. Kibble, G. Mackenzie, A. Rocher, *Soft Matter* **2011**, *7*, 4017.
[46] P. E. Jardine, W. T. Fraser, B. H. Lomax, W. D. Gosling, *J. Micropalaeontol.* **2015**, *34*, 139.
[47] S. Blackmore, R. B. Knox, *Microspores Evolution and Ontogeny: Evolution and Ontogeny*, Academic Press, London **2016**.
[48] E. Bormashenko, R. Grynyov, *Colloids Surf., B* **2012**, *97*, 171.
[49] D. Hetemi, J. Pinson, *Chem. Soc. Rev.* **2017**, *46*, 5701.
[50] K. Kasai, Y. Kimura, S. Miyata, *Mater. Sci. Eng. C* **2017**, *78*, 354.
[51] K. Uto, J. H. Tsui, C. A. DeForest, D.-H. Kim, *Prog. Polym. Sci.* **2017**, *65*, 53.
[52] N. Samsudin, Y. Z. H. Y. Hashim, M. A. Arifin, M. Mel, H. M. Salleh, I. Sopyan, D. N. Jimat, *Cytotechnology* **2017**, *69*, 601.
[53] D. Ge, Y. Li, L. Yang, Z. Fan, C. Liu, X. Zhang, *Thin Solid Films* **2011**, *519*, 5203.
[54] G. V. Lubarsky, M. R. Davidson, R. H. Bradley, *Appl. Surf. Sci.* **2004**, *227*, 268.
[55] P. E. Jardine, F. A. Abernethy, B. H. Lomax, W. D. Gosling, W. T. Fraser, *Rev. Palaeobot. Palynol.* **2017**, *238*, 1.
[56] P. E. Jardine, W. T. Fraser, B. H. Lomax, M. A. Sephton, T. M. Shanahan, C. S. Miller, W. D. Gosling, *Sci. Rep.* **2016**, *6*, 39269.
[57] H. Sénéchal, N. Visez, D. Charpin, Y. Shahali, G. Peltre, J.-P. Biolley, F. Lhuissier, R. Couderc, O. Yamada, A. Malrat-Domenge, *Sci. World J.* **2015**, *2015*, 94024.
[58] J. Wolters, M. Martens, *Bot. Rev.* **1987**, *53*, 372.
[59] E. Paoletti, L. Bellani, *Environ. Pollut.* **1990**, *67*, 279.
[60] O. Naas, M. Mendez, M. Quijada, S. Gosselin, J. Farah, A. Choukri, N. Visez, *Environ. Pollut.* **2016**, *214*, 816.
[61] M. J. Uddin, H. S. Gill, *J. Controlled Release* **2017**, *268*, 416.
[62] M. Saeed, M. Naveed, M. Arif, M. U. Kakar, R. Manzoor, M. E. A. El-Hack, M. Alagawany, R. Tiwari, R. Khandia, A. Munjal, *Biomed. Pharmacother.* **2017**, *95*, 1260.

[63] V. A. S. de Arruda, A. Vieria dos Santos, D. Figueiredo Sampaio, E. da Silva Araújo, A. L. de Castro Peixoto, M. L. F. Estevinho, L. Bicudo de Almeida-Muradian, *J. Apic. Res.* **2017**, *56*, 231.
[64] H. Bubert, J. Lambert, S. Steuernagel, F. Ahlers, R. Wiermann, *Z. Naturforsch. C Bio. Sci.* **2002**, *57*, 1035.
[65] J. S. Watson, M. A. Sephton, S. V. Sephton, S. Self, W. T. Fraser, B. H. Lomax, I. Gilmour, C. H. Wellman, D. J. Beerling, *Photochem. Photobiol. Sci.* **2007**, *6*, 689.
[66] R. M. Silverstein, F. X. Webster, D. J. Kiemle, D. L. Bryce, *Spectrometric identification of organic compounds*, John Wiley & Sons, New York **2014**.
[67] Z. Movasaghi, S. Rehman, D. I. ur Rehman, *Appl. Spectrosc. Rev.* **2008**, *43*, 134.
[68] F. Ahlers, H. Bubert, S. Steuernage, R. Wiermann, *Z. Naturforsch. C Bio. Sci.* **2000**, *55*, 129.
[69] M. Bağcıoğlu, B. Zimmermann, A. Kohler, *PloS One* **2015**, *10*, e0137899.
[70] R. J. Klein, D. A. Fischer, J. L. Lenhart, *Langmuir* **2008**, *24*, 8187.
[71] Y. Sakurai, N. Kawashima, Y. Tokuoka, *Colloid Polym. Sci.* **2017**, *295*, 413.
[72] A. M. a. Amat, A. Arques, M. A. Miranda, *Appl. Catal., B* **1999**, *23*, 205.
[73] D. Lehnert, B. Wehrle-Haller, C. David, U. Weiland, C. Ballestrem, B. A. Imhof, M. Bastmeyer, *J. Cell Sci.* **2004**, *117*, 41.
[74] K. Saha, Y. Mei, C. M. Reisterer, N. K. Pyzocha, J. Yang, J. Muffat, M. C. Davies, M. R. Alexander, R. Langer, D. G. Anderson, *Proc. Natal. Acad. Sci. USA* **2011**, *108*, 18714.
[75] D. Teare, N. Emmison, C. Ton-That, R. Bradley, *Langmuir* **2000**, *16*, 2818.